Transition mechanism in a shock wave boundary layer interaction

Moussa Diop

Aix Marseille Univ
CNRS, IUSTI
13453 Marseille cedex 13, France
moussa.diop.1@etu.univ-amu.fr

Sébastien Piponniau

Aix Marseille Univ
CNRS, IUSTI
13453 Marseille cedex 13, France
sebastien.piponniau@univ-amu.fr

Pierre Dupont

Aix Marseille Univ
CNRS, IUSTI
13453 Marseille cedex 13, France
pierre.dupont@univ-amu.fr

ABSTRACT

The spatial development of a transitional Oblique Shock Wave Interaction at Mach 1.68 is documented thanks to high resolution Laser Doppler Anemometer (LDA) and Hot Wire Anemometer (HWA) measurements. The amplifications of the velocity fluctuations along the transitional separated shear layer is found to follow an exponential growing. The time properties of these unsteadiness are characterized with external hot wire measurements.

1 Introduction

Since its first appearance in the 40s, shock-wave boundary layer interactions (SWBLI) have been widely studied numerically and experimentally, both with laminar or turbulent boundary layer. SWBLI is a physical phenomenon that appears in supersonic engines, such as at the extrados of a supersonic air-plane, in supersonic intakes or in over-expanded nozzles. It is known to generate thermal and aerodynamic loads that can be harmful for system, Erdem *et al.* (2013). It is also known to cause boundary layer separation when its intensity is high enough. Depending on whether the boundary layer is separated or not, the upstream state is laminar or turbulent, the topology of SWBLI can be very different.

A large part of SWBLI studies considered a turbulent boundary layer, and were realized using several geometries configuration, including *compression ramp* (Wu & Martin (2008)), *oblique shock wave* (Dupont *et al.* (2006) ; Touber & Sandham (2009)) and *normal shock wave* (Pirozzoli *et al.* (2009)). While pioneers investigations were mainly focused on spatial and pressure description, what have permitted a good understanding of flow organisation, nowadays, thanks to the improvement of metrology technique and the increase of computing capacity, authors focus their research on the source of the low frequency unsteadiness in separated turbulent SWBLI (Ganapathisubramani *et al.* (2007); Piponniau *et al.* (2009); Touber & Sandham (2008)). These studies have confirmed the existence of low frequency unsteadiness of the separated SWBLI, with a characteristic frequency of two order of magnitude lower than the characteristics frequencies of the incoming boundary layer. This low frequency is described to be potentially dangerous for engines since it can excites their eigen modes.

Compared to turbulent SWBLI, laminar ones have been less investigated. Nevertheless, they have recently gained interest since aeronautical industries are confronted to the challenging reduction of air-plane impact on the environment. In fact, reduction of greenhouse gaze can be achieved, in particular, by reducing air-plane drag. A solution may consist of the use of laminar profile at high altitude where favorables conditions (low Reynolds numbers) allow the boundary layer to stay laminar a long distance downstream of the leading edge, reducing dramatically the skin friction. Unfortunately, the boundary can separate easier than a turbulent boundary layer, when it sustains an adverse pressure gradient, and this causes worsening of aerodynamic performances. Furthermore, it is well established that such separated interactions exhibit low frequency unsteadiness (Sansica *et al.* (2016)) as do turbulent separated interactions. In addition, we know that laminar transition to turbulence is promoted when the boundary layer is separated (Giepman (2016)). Although, this allows the boundary layer to reattach, laminar transition to turbulent may contribute to increase more performances losses by increasing the drag.

Here, a transitional SWBLI at nominal Mach number 1.68 is considered. The unitary Reynolds number is $Re_u = 5.7 \times 10^6$. The flow is documented using Hot Wire Anemometer and high resolution Laser Doppler Anemometer. Thes paper is organized as follow. In section 2, we present the experimental set-up . Section 3 is devoted to the presentation of the LDA set-up. Then, we describe the time scales developing along the interaction in section 4, and finally a discussion about the transitional mechanism along the interaction is made section 5.

2 Experimental Set Up

Experiments are carried out in the hypo-turbulent supersonic wind tunnel of the IUSTI laboratory, at the Aix-Marseille University, France. This is a continuous facility with a closed-loop circuit. The nominal Mach number of the test section is $M = 1.68$, and the total pressure is of 0.4×10^5Pa. The turbulence intensity of the pressure fluctuations in the potential flow are as low as 0.4% at this stagnation pressure. The reflection of an oblique shock wave on a laminar supersonic boundary layer developing over a flat plate is considered. The model is composed of a flat plate of 175mm long. A sharp-edged shock generator is installed at 72mm downstream of the leading edge of the flat plate and at 30mm distance from the wall of the plate. The shock generator and the flat plate spans are as large as the wind tunnel test section. The origin of the abscissa x is taken at the leading edge of the flat plate. The flow deviation θ was fixed to 5°. A sketch of the experimental set-up is shown Figure 1.

The boundary layer which is developing along the flat plate has been controlled to be laminar Diop *et al.* (2016). For a theoretical laminar boundary, velocity profiles are self-similar:

$U/Ue = f(y\sqrt{Re_u/x})$, where Re_u is the unitary Reynolds number. Indeed, the boundary layer thickness evolves as :$\delta \propto \sqrt{x/Re_u}$. Figure 2 represents the mean velocity profiles obtained from LDA measurements, for positions ranging from 80mm to 160mm and for stagnation pressure from 0.4atm to 0.8atm, it means for Reynolds numbers Re_x from $0,448 \times 10^6$ to 0.919×10^6. As seen on the figure, boundary layer profiles are in a good agreement with the compressible Blasius profile obtained from StarCCM+ computation. The impingement location of the incident shock wave X_{imp} is at 107.3mm from the leading edge. At this location, the undisturbed boundary layer thickness is $\delta_{imp} = 0.9$mm and the displacement thickness is $\delta^*_{imp} = 0.4$mm. The upstream influence of the interaction X_0 has been defined as the extrapolation down to the wall of the inflection point of the pressure rise across the compression waves (derived from Pitot measurements at 5mm from the wall, Figure 9). This position can be seen as the mean position of the separation point. At this location, the undisturbed boundary layer thickness is $\delta_0 = 0.7$mm and the displacement thickness is $\delta^*_0 = 0.3$mm. The length of the interaction L, defined as the distance between X_0 and X_{imp}, is 43.7mm. The non-dimensional longitudinal coordinate is $X^* = (X - X_{imp})/L$. The position of the incident shock at the wall is then $X^* = 0$ and the compression waves are centered around $X^* = -1$.

3 High resolution LDA measurements

The LDA probe volume diameter Φ used for results presented Figure 2 is 75μm, Diop *et al.* (2016). It has to be compared with the

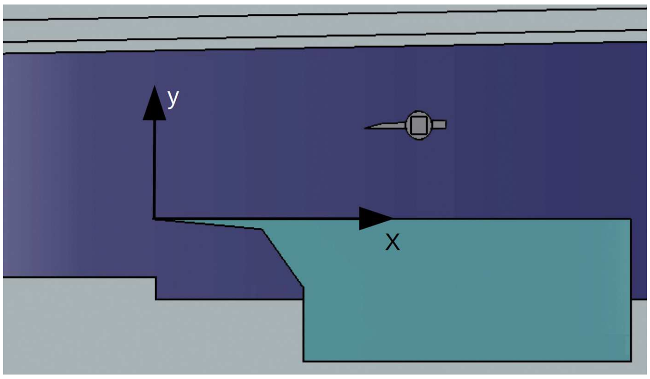

Figure 1. Test section with model

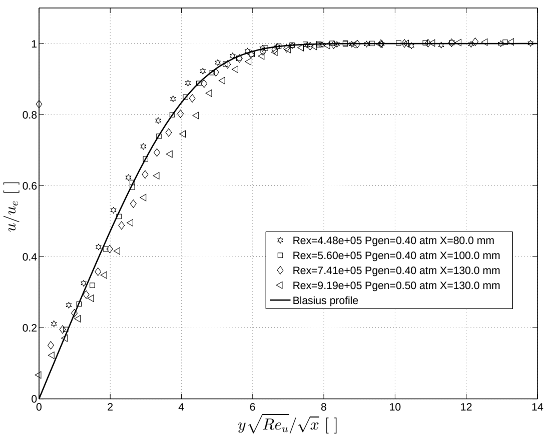

Figure 2. Velocity profiles in normalized representation - LDA meaurements. From Diop *et al.* (2016)

thickness of the boundary layer at the section X_0 which is as small as 700μm. Therefore, the velocity gradient across the diameter of the probe volume cannot be neglected. Based on classical models to take into account the velocity gradient inside the probe volume Durst *et al.* (1976), an analytical expression of the bias measurements was derived.

We consider a measurement volume of a diameter of Φ inside the boundary layer at a position y from the wall. Thanks to the small size of the the measurement volume, we can assume with little bias that the velocity distribution inside the probe volume is linear :

$$U(\xi) = U_y + \alpha\xi \tag{1}$$

where U_y denotes the mean velocity measured at the center of the probe volume, $-\Phi/2 \leq \xi \leq +\Phi/2$ and α is the slope of the linear velocity profile inside the probe. We assume that seeding particles passing through the probe volume are equally distributed inside de volume such that the probability density of a particle to pass at a position ξ inside the volume is given by :

$$p(\xi) = \frac{1}{\Phi} \; with \; \int_{-\Phi/2}^{+\Phi/2} p(\xi)d\xi = 1 \tag{2}$$

With these assumptions we can evaluate the artificial variance of velocity introduced by the velocity gradient inside the measurement volume. Considering $U(\xi)$ as a random variable, its variance can be expressed using the definition of the expectancy $E(U)$ through :

$$Var(U) = E(U^2) - (E(U))^2 \tag{3}$$

Values of $E(U^2)$ and $(E(U))^2$ are obtained like :

$$E(U) = \int_{-\Phi/2}^{+\Phi/2} U(\xi)p(\xi)d\xi = \int_{-\Phi/2}^{+\Phi/2} (U_y + \alpha\xi)p(\xi)d\xi = U_y \tag{4}$$

$$E(U^2) = \int_{-\Phi/2}^{+\Phi/2} U(\xi)^2 p(\xi)d\xi = \int_{-\Phi/2}^{+\Phi/2} (U_y + \alpha\xi)^2 p(\xi)d\xi \tag{5}$$

$$(E(U))^2 = U_y^2 \text{ and } E(U^2) = U_y^2 + \alpha^2\frac{\Phi^2}{12} \tag{6}$$

Then, the RMS velocity fluctuations is:

$$u' = \sqrt{Var(U)} = \sqrt{\alpha^2\frac{\Phi^2}{12}} \text{ and } \frac{u'}{U_e} = \frac{\Phi}{2\sqrt{3}}\frac{|\alpha|}{U_e} \tag{7}$$

In laminar boundary layer, the slope α is constant in the vicinity of the wall up to $U/U_e = 0.6$, see Figure 2, but inside the separated interaction, the slope is no longer constant due to reverse flow, and has to be evaluated. We can estimate α as followed, with subscript i designating the current position of the measurement volume and U_i the velocity at this position.

$$|\alpha| = \frac{1}{2}\left(\left|\frac{U_i - U_{i-1}}{y_i - y_{i-1}}\right| + \left|\frac{U_{i+1} - U_i}{y_{i-1} - y_i}\right|\right) \tag{8}$$

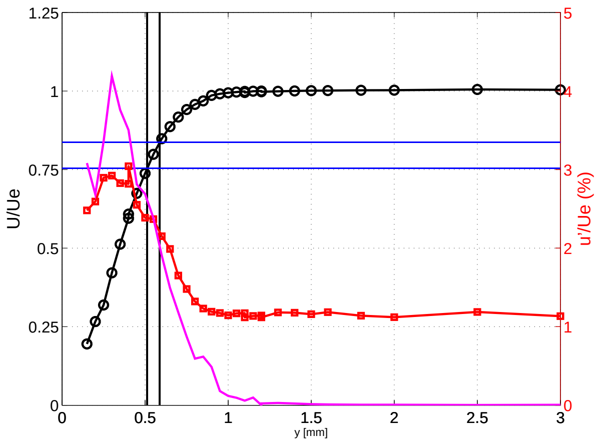

Figure 3. Mean (▬) and turbulence intensity (▬) measured in the upstream boundary layer vs modelling of the probe volume integration effects (▬), 75μm probe volume

The apparent intensity of velocity fluctuations is then

$$\frac{u'}{U_e} = \frac{\Phi}{2\sqrt{3}} * \frac{1}{2}\left(\left|\frac{U_i - U_{i-1}}{y_i - y_{i-1}}\right| + \left|\frac{U_{i+1} - U_i}{y_{i+1} - y_i}\right|\right) \tag{9}$$

The equation 9 is compared to the intensity of velocity fluctuations derived from the LDA measurements in the initial part of the laminar boundary layer (see Figure 3). It describes accurately the present measurements in the upstream laminar boundary layer for the 75μm probe volume diameter used for the mean velocity measurements .

Equation 9 shows that a reduction of the measurement volume diameter of the LDA entails a diminishing of the apparent intensity of velocity fluctuations. We undertake a reduction of the volume diameter from 75μm to 38μm. The volume diameter of the probe volume and the fringes wavelength are given by :

$$\Phi = \frac{d_f}{cos(\theta/2)} \; ; \; \delta_f = \frac{\lambda}{2sin(\theta/2)} \tag{10}$$

where $d_f = \frac{4f\lambda}{\pi G d_I}$ is the beam waist and θ the angle between the two beams; f is the focal length, λ the wave length of the emitted beam, d_I is the beam waist upstream of the front lens and G designates the beam-expansion factor. Reduction of the probe volume diameter is realized by increasing the beam expansion factor G, which is done by connecting in series two beam-expanders such that the resulting beam-expansion factor is $G^2 = 3.92$.

Nevertheless, the set up of the LDA system, particularly when defining the probe diameter need to take into account the cut-off frequency of the photomultiplier which is about 180MHz. The maximum Doppler frequency has to be fixed to a much lower value than 180MHz in order to avoid signal attenuation. In flows with separation, a Bragg cell is used to resolve negatives velocities. It introduces a shift frequency ($f_{Bragg} = 40$ Mhz) that increases the Doppler frequency. If we limit the Doppler frequency value at $f_{Dmax} = 100 - 120$ MHz, as the external velocity is $U_e = 450ms^{-1}$, the shortest inter-fringe which can be used should be $\delta_{f_{min}} = U_e/(f_{D_{max}} - f_{Bragg}) = 5.6 - 7.5\mu$m.

The distance between beams upstream of the beam-expander has been fixed at 11 mm. The resulting distance between the two beams

Table 1. LDA characteristics

Φ [μ m]	Beam spacing [mm]	Beam expander ratio	l [mm]	Fringe spacing [μm]	F_{max} [MHz]
75	19.2	1.98	1.9	6.70	110
38	11	3.92	0.66	5.97	117

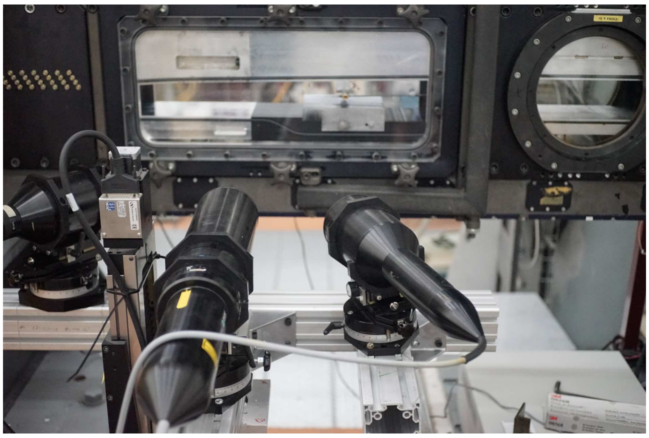

Figure 4. 38μm probe volume LDA set-up

downstream of the beam-expander is $\simeq$ 43mm. The converging lens is of 500 mm. Main parameters of the 75μm and 38μm LDA settings are reported Table 1. The fringe spacing is nearly constant for both set-ups, and is about 7μm. This correspond to maximum Doppler frequency of about 110MHz. Notice that the number of fringes is then reduced between the measurement volume of 75μm and that of 38μm. The uncertainty on the Doppler frequency evaluation depends on the number of fringes (N) inside the probe volume Pfeifer (1976),p1-8:

$$\frac{\Delta f_D}{f_D} = \frac{\sqrt{2}}{\pi}\frac{1}{N} \tag{11}$$

This uncertainty in the frequency evaluation introduces an additional bias error to the apparent intensity of velocity fluctuations, since the Doppler frequency is linked to the velocity through $U = \delta_f(f_D - f_{Bragg})$.

Only one beam expander is used for the receiving optic. Thus, the pin-hole is quite larger than the probe volume, and, since we are in an off-axis configuration, the probe volume has an apparent length long enough to optimize the reception data rate. The 38μm LDA installation is shown Figure 4.

This new LDA set up is used to achieved measurement of the longitudinal velocity fluctuations along the interaction. For the stations downstream from the separation point ($X^* > -1$), RMS values become significantly larger than the apparent turbulence and accurate measurements can be derived if the measurements are corrected from the artificial turbulence. RMS profiles measured along the interaction are shown Figure 5. The maxima of the RMS of the velocity fluctuations are increasing along the interaction: their location and amplitudes are reported on the figure (cyan and magenta lines respectively).

The longitudinal evolution of the maxima RMS longitudinal velocity fluctuations are reported Figure 6. Their amplitude is found

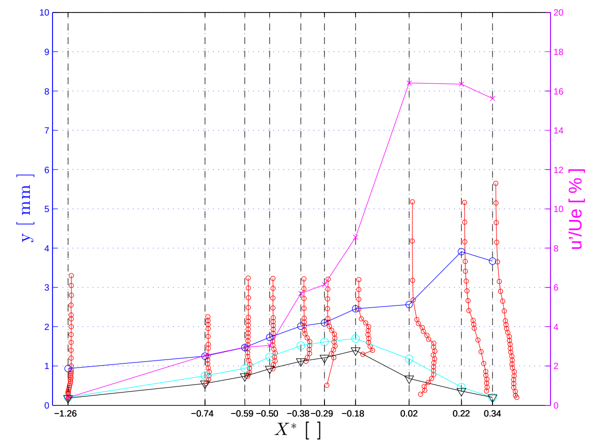

Figure 5. Turbulent longitudinal velocity LDA measurements along the interaction with the 38μm probe volume.

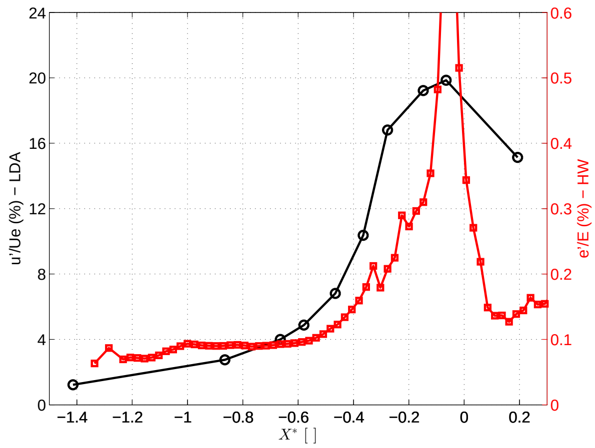

Figure 7. Qualitative comparison between the LDA measurements and HW measurements performed at 5mm from the wall.

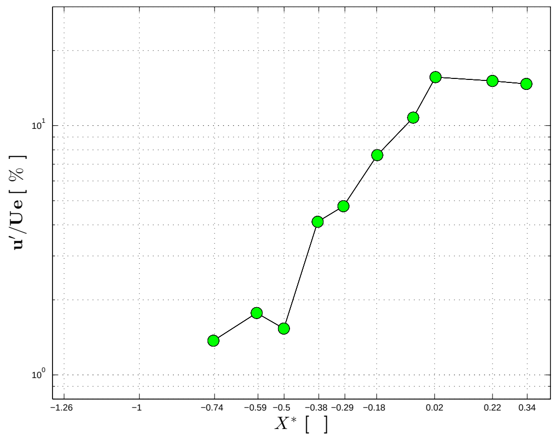

Figure 6. Longitudinal evolution of the maxima of RMS along the interaction.

.

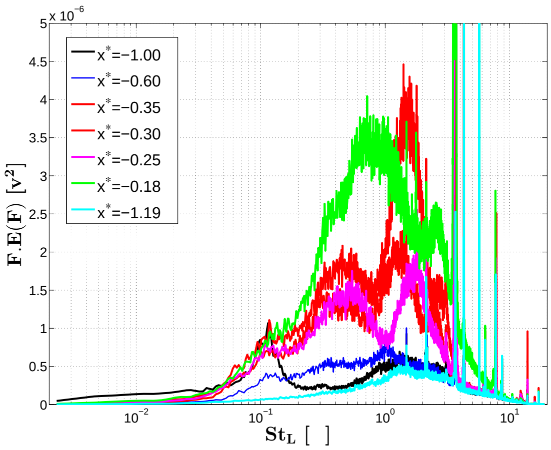

Figure 8. Longitudinal evolution of PSD of the pressure radiated fluctuations (hot wire measurements) .

.

to increase along the interaction: it varies from about 1% of the external velocity U_e (which is the noise level of these LDA measurements) to a saturation level of about $0.17U_e$ near the incident shock impingement location. In the initial part of the interaction ($-1 < X^* < -0.5$), the amplitude of the velocity of fluctuations are too low to be resolved from the present LDA measurements. The velocity profiles measured downstream from the interaction show that the boundary layer is no longer laminar. The incompressible form factor for a laminar boundary layer is of (2.61). In this section it is of 1.62, similar to turbulent profiles. Nevertheless, no clearly defined log-law region has been observed: the boundary layer is still in a transitional state. In this downstream region, large velocity fluctuations are observed, higher than expected for a classical turbulent profiles: at this position (about 30 displacement thickness δ^*_{imp} downstream from the impingement location), the flow is still relaxing.

4 Time scales developed along the interaction

LDA measurements provides new results on the velocity fluctuations inside the separated shear layer. Unfortunately, the data-rates were not high enough (typically around 1 to 5kHz) to resolve accurately their time properties. Therefore, hot wire measurements have been achieved in order to derive the Power Spectral Densities of the momentum fluctuations. As measurements inside the separated shear layer were of limited accuracy (probe vibrations, transonic effects, recirculating flows), we measured over the shear layer ($y = 5mm$) the radiated pressure perturbations (Smits & Dussauge (2006), pp25-32 et p125, Agostini *et al.* (2012), Jaunet *et al.* (2014)). The locations of HWA measurement positions are sketched figure 9. The measured intensity of voltage fluctuations along the interaction is compared to the longitudinal evolution of the maxima RMS velocity fluctuations figure 7. On this figure, the location of the hot wire measurements were corrected from the angle of the characteristics for a Mach number of 1.68 to match with LDA measurement positions. Similar evolution are obtained, with a large increase of the radiated fluctuations in the second part of the interaction ($-0.5 < X^*$) as for the LDA measurements. HWA measurements are used to characterize the times scales developing along the interaction.

The pre-multiplied PSD are plotted vs the Strouhal number $S_L = fL/U_e$ along the interaction Figure 8. Curves are colored with respect to measurement positions as on Figure 9. Results presented Figure 8 highlight the unsteadiness of the compression waves

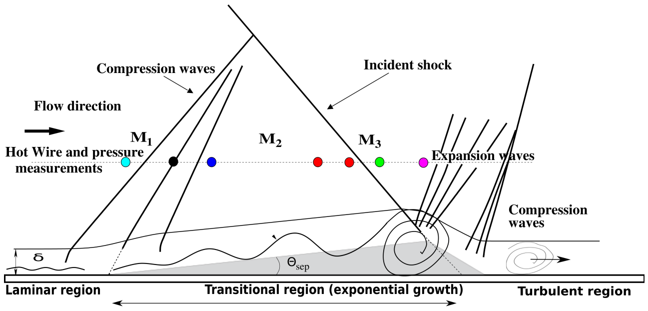

Figure 9. Sketch of the transition development along the interaction.

and allow to identify their mean characteristic frequency which is around $S_L = 0.12, f = 1.5$kHz. Downstream from the compression waves, a global amplification of perturbations is observed for Strouhal number ranging from 0.1 to 3. These scales are amplified all along the interaction, with a maximum of amplitude around $S_L = 1.48, f = 15$kHz. Another characteristic amplified Strouhal number can be observed on the figure : intermediated frequencies around $S_L = 0.5, f = 5$kHz. In our transitional interaction case, the Reynolds number at separation point is $Re_{X_0} = 365000$. Hot wire measurements inside the upstream laminar boundary layer exhibit so low level that growing of any characteristics times scales of the boundary layer was above measurement uncertainty. Nevertheless, for higher Reynolds number $Re_x > 900000$, Power Spectrum Density of laminar boundary layer perturbations highlights amplification of bandwidth frequency around $S_L = 1.48, f = 15$kHz. This suggest that the amplified modes in the interaction, around $S_L = 1.48$, have to be related to the unsteady modes of upstream laminar boundary layer.

5 Transitional mechanism along the interaction

A global overview of the transition process along the interaction can be inferred from the present measurements. It is reported Figure 9. The upstream flow is a laminar boundary layer. At the separation point ($X^* = -1$), compression waves are developing and the decelerated shear layer is growing down to the apex location (around $X^* = -0.2$). The flow deviation at the separation point has been derived from mean external pressure measurements. Using the pressure jump through the compression waves and the upstream external Mach number, we deduce the wedge angle producing the same pressure jump. A deviation of 2°was evaluated: the initial flow deviation is less than the half of the imposed flow deviation. These results suggest that the pressure field in vicinity of the separation depends only on the upstream conditions. Such behavior was proposed in the Free Interaction Theory Chapman *et al.* (1957), where the initial pressure rise is given by:

$$\frac{p(\bar{x}) - p_1}{p_1} = \frac{1}{2}\gamma M_1^2 \times F(\bar{x}) \sqrt{\frac{2C_{f1}}{(M_1^2 - 1)^{1/2}}} \qquad (12)$$

p_1, M_1, C_{f_1} being respectively the pressure, the Mach number and the skin friction coefficient measured at the beginning of the interaction. The universal function $F(\bar{x})$ depend only on the initial state of the upstream boundary layer and is equal to 1.5 downstream of the separation point for upstream laminar flow. This relations leads to an equivalent flow deviation of 2°2 for the present experimental conditions, in very good agreement with the experimental value.

In the upstream laminar boundary layer, unsteady modes are developing, with very low amplitude for such Reynolds number ($Re_{X_0} = 365000$). These modes correspond to high frequencies (about 15kHz, $S_L = 1.5$ in our case). They are strongly amplified along the separated shear layer, with an exponential growth, up to a saturation level which corresponds to transitional-turbulent values. This increase dramatically the momentum transfer across the shear layer and the flow is reattaching. The large scales developed along the interaction are shed downstream from the reattachment. This is similar to results of Sansica *et al.* (2016) who forced a separated interaction with unstable modes of the separated bubble obtained by Linear Stability Theory (LST) and found these unstable modes to experience a weak growth along the attached boundary layer and a strong growth inside the bubble that may lead to a non-linear interaction and then to turbulence break-down. Therefore, it seems that, for this range of frequencies, the transitional SWBLI can be considered as a noise amplifier.

The downstream boundary layer is out of equilibrium, with maxima of velocity fluctuations far from the wall in the middle of the layer. This is very similar to what is observed in separated turbulent shock wave boundary layer interactions, despite significant differences between the Strouhal number (0.5 and 1.5 respectively for the turbulent and transitional cases).

Over imposed on these high frequency unsteadiness, very low frequencies are observed all along the interaction. They correspond to dimensionless frequencies around $S_L = 0.12$ and are clearly associated with low frequency motions of the initial compression waves. This value differs significantly from the dimensionless low frequencies associated to separated shock of turbulent interactions, which is around $S_L = 0.03$. In Piponniau *et al.* (2009), it was suggested that the low frequency unsteadiness in SWBLI should vary as the aspect ratio L/h of the interaction. The aspect ratio of transitional and turbulent SWBLI can be approximated from the flow deviation θ_{sep} at the separation point: $L/h \simeq 1/tan(\theta_{sep})$. In our transitional interaction configuration, a flow deviation angle of 2° has been obtained, against around 10° flow deviation angle for turbulent SWBLI (Green (1970)). Then a ratio of about $(L/h)_{tr}/(L/h)_{turb} = tan(10)/tan(2)$ can be expected between the low frequency transitional and turbulent Strouhal numbers. Thus, the dimensionless low frequency of SWBLI for turbulent and laminar cases should be related as $(S_L)_{tr} = tan(10)/tan(2) \times (S_L)_{turb} = 0.15$. The expected Strouhal number is approximatively equal to the one found in our configuration. Therefore, present measurements seem to confirm the low frequency dependence on the aspect ratio of the interaction. Otherwise, perturbations through the interaction exhibit a medium frequency around $S_L = 0.5, f = 5$kHz which is amplified along the interaction. The same Strouhal number have been found in turbulent SWBLI, and has been related to convective structures developing along the shear layer with convective velocity of $U_c/U_e \simeq 0.3$ and characteristic wavelengths as $\lambda/L \simeq 0.6$, Dupont *et al.* (2006). Nevertheless, the very large aspect ratios in transitional cases suggest that such assumption is not more relevant, as such unsteadiness would involve wavelength of about 100 initial boundary layer displacement thickness. Additional elements, as phase velocity, are clearly required to analyze these intermediate time scales.

6 Conclusion

We considered a transitional SWBLI at free Mach number 1.68 and stagnation pressure $Po = 0.4$atm. A LDA set-up, corresponding to a probe volume diameter of 38μm, has been defined. It allows to reduce the apparent velocity fluctuations. Perturbations along the separated shear layer are found to evolve exponentially, and may be responsible for laminar-turbulent transition that takes place inside

the bubble. Hot wire measurements of the pressure fluctuations radiated from the shear layer show that this transition process results from the contribution of several bandwidth frequencies. The high frequencies correspond to a strong amplification along the separated shear layer of the upstream perturbations which are developing in the upstream laminar boundary layer. They are amplified up to a saturation level which defines the transition to turbulence of the flow: at this station, the flow is reattaching. For this range of frequencies, the interaction can be considered as a noise amplifier.
Superimposed are low and intermediate frequencies. The low ones can be compared with classical results in turbulent separated SWBLI if the differences between transitional and turbulent aspect ratio are considered. Intermediate frequencies are still to be describe and need further analysis

Acknowledgments

This work received financial support by the TFAST Project of the European Commission's 7th Framework Programme 265455 and the Labex MEC. Their support is gratefully acknowledged.

REFERENCES

Agostini, L., Larchevêque, L., Dupont, P., Debiève, J.F. & Dussauge, J.P. 2012 Zones of influence and shock motion in a shock boundary layer interaction. *AIAA Journal* **50** (-6), 1377–1387.

Chapman, D. R., Kuehn, D. M. & Larson, H. K. 1957 Investigation of separated flow in supersonic and subsonic streams with emphasis of the effect of transition. *Tech. Rep.*.

Diop, M., Piponniau, S. & Dupont, P. 2016 *On the length and time scales of a laminar shock wave boundary layer interaction*. American Institute of Aeronautics and Astronautics.

Dupont, P., Haddad, C. & Debiève, J. F. 2006 Space and time organization in a shock induced boundary layer. *Journal of Fluid Mechanics* **559**, 255–277.

Durst, F., Melling, A. & Whitelaw, J. H. 1976 *Principles and Practice of Laser-Doppler Anemometry*.

Erdem, E., Kontis, K. & Johnstone, E. 2013 Experiments on transitional shock wave–boundary layer interactions at Mach 5 . *Experiments in Fluids* .

Ganapathisubramani, B., Clemens, N. T. & Dolling, D. S. 2007 Effects of upstream boundary layer on the unsteadiness of shock–induced separation. *Journal of Fluid Mechanics* **585**, 369–394.

Giepman, R. 2016 Flow Control for Oblique Shock Wave Reflections. PhD thesis, Delft University of Technology.

Green, J.E. 1970 Reflexion of an oblique shock wave by a turbulent boundary layer. *Journal of Fluid Mechanics* **40**, 81–95.

Jaunet, V., Debiève, J. F. & Dupont, P. 2014 Length Scales and Time Scales of a Heated Shock-Wave/Boundary-Layer Interaction. *AIAA Journal* pp. 1–9.

Pfeifer, H. J. 1976 Review on high speed applications of laser anemometry in France and Germany. *Applications of Non-Intrusive Instrumentation in Fluid Flow Research*. *Tech. Rep.* AGARDograph-CP-193.

Piponniau, S., Dussauge, J. P., Debiève, J. F. & Dupont, P. 2009 A simple model for low-frequency unsteadiness in shock-induced separation. *Journal of Fluid Mechanics* **629**, 87–108.

Pirozzoli, S., Beer, A., Bernardini, M. & Grasso, F. 2009 Computational analysis of impinging shock–wave boundary layer interaction under conditions of incipient separation. *Shock Waves* **19** (6), 487–497.

Sansica, A., Sandham, N. D. & Hu, Z. 2016 Instability and low-frequency unsteadiness in a shock-induced laminar separation bubble. *J. Fluid Mech.* **798**, 5–26.

Smits, A. J. & Dussauge, J. P. 2006 *Turbulent shear layers in supersonic flow*, 2nd edn. AIP Press.

Touber, E. & Sandham, N. D. 2008 Oblique shock impinging on a turbulent boundary layer: low-frequency mechanisms. In *38th AIAA Fluid Dynamics Conference, Seattle, Washington, USA*.

Touber, E. & Sandham, N. D. 2009 Comparison of three large–eddy simulations of shock–induced turbulent separation bubbles. *Shock Waves* **19** (6), 469–478.

Wu, M. & Martin, M. P. 2008 Analysis of shock motion in shock-wave and turbulent boundary layer interaction using direct numerical simulation data. *Journal of Fluid Mechanics* **594**, 71–83.